Journal of Materials Chemistry A

Accepted Manuscript

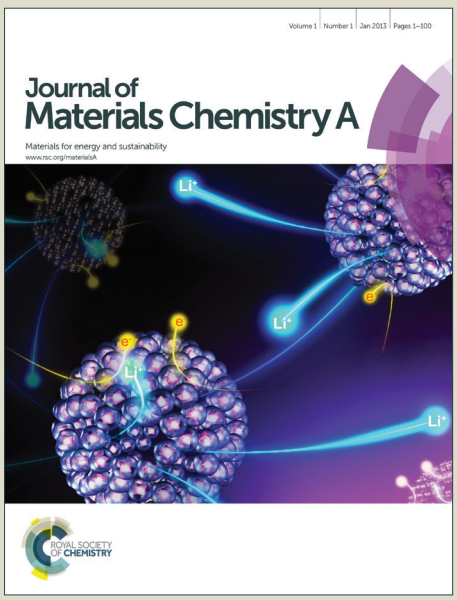

ROYAL SOCIETY OF CHEMISTRY

www.rsc.org/materialsA

Optimisation of diketopyrrolopyrrole:fullerene solar cell performance through control of polymer molecular weight and thermal annealing.

Zhenggang Huang, Elisa Collado Fregoso, Stoichko Dimitrov, Pabitra Shakya Tuladhar, Ying Woan Soon, Hugo Bronstein, Iain Meager, Weimin Zhang, Iain McCulloch, James R. Durrant*

Centre for Plastic Electonics, Department of Chemistry, Imperial College London, London SW7 2AZ, U.K.

Correspondence email: j.durrant@imperial.ac.uk

Table of content entry

Performance of bulk heterojunction solar cells based on a novel donor polymer DPP-TT-T was optimised using two different approaches, namely tuning molecular weight and thermal annealing.

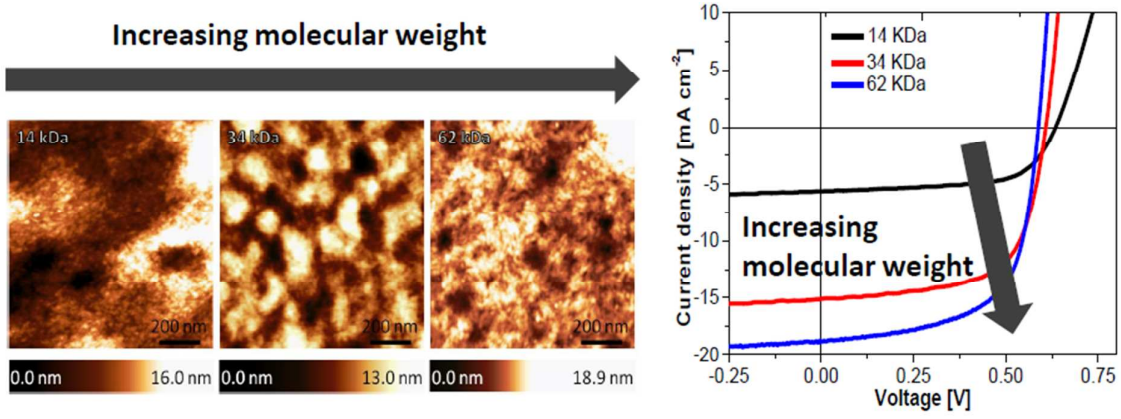

Abstract

Poly-Thieno[3,2*b*]thiophene-Diketopyrrolopyrrole-co-Thiophene (DPP-TT-T) is a promising low bandgap donor polymer for organic solar cells. In this study we employ two different approaches to improve the device efficiency via optimisation of the morphology of the active layer: tuning of the molecular weight of the polymer and thermal annealing. In the former case, a higher molecular weight was found to yield a more intermixed morphology, resulting in enhanced exciton dissociation and charge separation process, as confirmed by atomic force microscopy, and photoluminescence and transient absorption spectroscopies. In the later case, thermal annealing prior to metal electrode deposition increased the photon conversion efficiency to as high as 6.6%, with this enhanced efficiency being maintained even with prolonged annealing (240 hours at 80 °C). This enhancement in performance with thermal annealing was correlated with increased polymer crystallinity.

Introduction

Organic photovoltaic (OPV) cells based on polymer:fullerene blends have improved significantly in terms of power conversion efficiency in recent years.[1, 2] One of the key drivers for this improvement has been the development of lower band gap polymers which are able to harvest more photons under solar exposure than traditional polymers such as P3HT. In this regard, diketopyrrolopyrrole (DPP) containing polymers are attracting particular interest due to their low optical band gaps (E_g as low as 1.4 eV) , solution processibility and high hole mobilities (FET mobilities up to 1.42 $cm^2 V^{-1} S^{-1}$).[3, 4] One of the most promising polymers in this family is poly-thieno[3,2*b*]thiophene-Diketopyrrolopyrrole-co-Thiophene (DPP-TT-TDPP-TT-T, Figure 1), with DPP-TT-TDPP-TT-T based devices exhibiting efficient photon-to-charge conversion extending up to 850 nm, and an initial power conversion efficiency (PCE) under solar irradiation of 5.4% .[5,6] The efficiency has been recently improved to 7.3% by modifying the side chain attached to the polymer.[7]

The efficiency of polymer:fullerene based organic solar cells is strongly dependent upon not only the selection of suitable donor polymers and acceptor fullerenes, but also upon the details of the material synthesis and film processing. Such dependencies have been most widely considered for the most established material system, poly(3-hexylthiophene) (P3HT): [6,6]-phenyl C_{61}-butyric acid methylester ($PC_{61}BM$), although the overall efficiency of this system is limited by its relatively large optical bandgap and the large energy offset employed to drive charge separation.[8, 9] In this study, we focus upon two such dependencies, polymer molecular weight and thermal annealing following film deposition, for devices based upon blends of the donor polymer DPP-TT-TDPP-TT-T with $PC_{71}BM$. Whilst both optimisation of polymer molecular weight and the application of thermal annealing have shown to be highly

effective in optimising device performance for P3HT:PCBM solar cells, such dependencies have received relatively little attention for the more recently developed, higher efficiency blend systems. In this regard, DPP-TT-TDPP-TT-T is particularly interesting as it exhibits a similar degree of crystallinity to P3HT,[10] suggesting that optimisation strategies shown to be effective for P3HT may also be potentially relevant to DPP-TT-TDPP-TT-T based devices.

In terms of molecular weight dependencies, studies to date have primarily focused on P3HT, with more limited studies of the alternative, more amorphous polymers MEH-PPV and PCDTBT.[11, 12, 13, 14] It has generally been observed that increasing polymer molecular weight improves the short circuit current and photon conversion efficiency of the corresponding devices.[11, 12, 13, 14] Early studies generally attributed the improvement in device performance to either a red shift in polymer absorption[15, 16] or increase in polymer mobility[11-13] at high molecular weight. For example, Schilinsky *et al*. reported improvements in performance of P3HT:PCBM based device as the polymer molecular weight (M_n) was changed from 2.2 kDa to 19 kDa, which was attributed to anincrease in polymer charge carrier mobility.[11] On the other hand, there is an increasing number of studies highlighting that the key to better performance with higher polymer molecular weight is improved morphology of the polymer:fullerene active layer.[17-19] In this regard, Nicolet *et al*. have reported that the device performance of P3HT:PCBM can be further improved until the M_n of P3HT reaches 60 kDa.[17] The improvement is believed to be due to better interconnectivity as well as finer mixing of P3HT and PCBM at high polymer molecular weight. In parallel, Janssen *et al.* have also reported the performance of a DPP-containing polymer based device can be improved by increasing the polymer molecular weight, attributed to the lower degree of phase segregation in the active layer.[20, 21] Later, Westacott *et al*. have suggested that the better

polymer:fullerene miscibility is a result of the larger portion of polymer amorphous phase offered by the high molecular weight P3HT.[18]

A range of annealing strategies have been employed to optimise the performance of P3HT:PCBM solar cells, including in particular thermal annealing before or, preferably, after electrode deposition.[11, 22] In this approach, the P3HT:PCBM blend morphology obtained from spin casting is allowed to rearrange itself towards thermodynamic equilibrium via thermal annealing, associated with an increase in P3HT crystallinity and more favourable phase segregation and domain structure. These changes in crystallinity and film microstructure have been suggested to increase charge separation efficiency, and also reduce non-geminate recombination losses, thereby increasing device efficiency.[22, 23] For such post-deposition treatments, the annealing temperature and duration needs to be controlled in order to obtain the most optimised device efficiency.[24] An additional consideration is whether annealing is performed before or after anode deposition ('pre-annealing' and 'post-annealing' respectively). For P3HT:PCBM devices, post-annealing has typically been reported to result in optimum device performance, dependent upon the details of device (and particularly electrode) composition. [24,25, 26]

Whilst studied in detail for P3HT:PCBM blends, there are relatively few studies on the use of molecular weight optimisation or thermal annealing to optimise device performance for other polymer:fullerene blends employed in OPV cell's. Indeed for most other blend systems, thermal annealing has been found to degrade device performance.[27, 28, 29, 30] As such, it is unclear whether these two device optimisation strategies are applicable to OPV's apart from those based on P3HT. We report herein the application of these two procedures to DPP-TT-TDPP-TT-T based device optimization, complimenting the approach we have

reported recently on optimising the polymer side chain.[7] Following these procedures, we are able to enhance device efficiency to 6.6% PCE, compared to 5.4% reported previously.[5] Insights into the origins of these performance enhancements were gained through a range of structural and functional characterisation assays.

Experimental

Material preparation

DPP-TT-TDPP-TT-T was prepared as previously reported, with the chemical structure shown in Figure 1.[5] The polymer was then fractionated using recycling gel permeation chromatography using chlorobenzene as a solvent and an Agilent PL gel 10µm MIXED-D column allowing the isolation of four different molecular weight fractions.[31] Three of these isolated molecular weights were employed for device fabrication: Fraction 1 (M_n = 62 kDa, PDI 1.9), Fraction 2 (M_n = 34 kDa, PDI 1.8), Fraction 3 (M_n =14 kDa, PDI = 1.9). The two batches of DPP-TT-TDPP-TT-T employed for the thermal annealing study have molecular weight of M_n ~17 kDa (PDI 6.4) and M_n ~ 35 kDa (PDI 4.3) respectively.

Device fabrication

All the OPV devices present in this paper have a 'conventional' device configuration that consisted of ITO/PEDOT:PSS/polymer:$PC_{71}BM$/Ca/Al. Glass substrates which were pre-coated with ITO were cleaned in detergent, distilled water, acetone and isopropanol under sonication sequentially for 15 minutes each. The substrates were then dried using nitrogen gun and then underwent ultraviolet ozone plasma treatment for 7 minutes. PEDOT:PSS solution was spin-casted onto the ITO substrates to give rise to ~ 30 nm PEDOT:PSS layers,

which were baked at 150 °C for 20 minutes before the introduction of the active layers. The active layer solutions had a 1:2 (polymer:$PC_{71}BM$) weight ratio in a binary solvent system (chloroform:dichlorobenzene 4:1) with overall polymer and fullerene concentration of 15 mg/ml for 14 kDa and 34 kDa fractions. The 62 kDa fraction exhibited poorer solubility and therefore the concentration of the corresponding solution was reduced to 7.5 mg ml^{-1}. The thicknesses of the spin cast active layers using such solutions were found to be around 80 nm. Then, a 25 nm thick Ca and 150 nm thick Al layers were deposited under high vacuum (2 $\times$ 10^{-6} mbar). For the thermal annealing approach, the active layers were annealed on a hot plate under nitrogen either prior to or after the cathode deposition. The annealing temperature and period are specified in section 3.

Instrumentation

JV characterisation

Devices performance measurements (active area 0.045 cm^2) were carried out in nitrogen environment. Current-density-voltage (J-V) curves were measured while the devices were exposed to light from a 150 W Xenon lamp filtered to simulate AM 1.5. The current passing through the devices was measured using a Keithley source meter while the voltage bias across the devices was varied. External quantum efficiency (EQE) of the devices was measured using a 100 W tungsten halogen lamp with a monochromator, as reported previously.[5] Spectral mismatch factors were extracted from the EQE measurement to correct the results obtained from the J-V measurements.

Spectroscopy

Transient absorption data was collected by a nano- to millisecond transient absorption set-up, as described elsewhere.[10] For the present experiment, excitation pulses were generated by a Nd:YAG-pumped optical parametric oscillator Opolette 355-LD (Opotek Inc.) with wavelength set at 800 nm. Excitation with low intensity (2 μJ cm^{-2}) was used to make sure the charge density in the thin films is on a comparable scale of those in devices under solar irradiation (10^{17} - 10^{18} cm^{-3}). When the experiment was repeated under oxygen atmosphere no visible differences were observed, showing that negligible long lived triplet generation. All transients are corrected for film fractional absorption ($1-10^{-abs}$) and could be fit to power law decays.

Photoluminescence spectra were measured with a Fluorolog-3 spectrofluorometer (Horiba Jobin Yvon) under air, uncorrected for spectrometer spectral response (which drops off towards 800 nm).

Atomic Force microscopy was performed on a 5500 AFM from Agilent Technology in tapping mode under air.

Wide angle X-ray scattering (WAXS): Samples for WAXS measurements were prepared in a drop-casting manner using solutions which are the same as those used for device fabrication. The measurements were carried out with a PANALYTICAL X'PERT-PRO Materials Research Diffractormeters (MRD) which has a nickel-filter Cu $K\alpha_1$ beam and a X' CELERATOR detector, using a current of 40 mA and an accelerating voltage of 40kV. Control data with P3HT employed purchased from Sigma with M_n ~ 35 kDa, pdi ~ 2, used as received, drop cast from a 10 mg/ml solution in dichlorobenzene.

Results

Effect of DPP-TT-TDPP-TT-T molecular weight

*Materials characterisation***.** The M_n of the DPP-TT-T fractions used for our study were 14 kDa, 34 kDa and 62 kDa respectively. In order to investigate the correlation between polymer molecular weight and crystallinity, wide angle X-ray scattering (WAXS) was used as an indicator for the crystallinity of drop cast pristine polymer films (Figure 2) in out-of-plane direction. In this Figure, the strong peaks at q ~ 0.3 $Å^{-1}$ are assigned to lamellar packing whilst the relatively weak peaks at q ~ 1.7 $Å^{-1}$ are assigned to π-π stacking. The degree of material crystallinity can be assayed by calculating the corresponding diffraction strengths , as shown in Table 1, defined as integration of the WAXS peaks following to previous studies.[10, 32] It is apparent that DPP-TT-T exhibits an increase in the degree of order for π-π stacking but a decrease in the degree of order for lamellar stacking as the molecular weight is increased. The total peak integration decreases as molecular weight is increased, implying a drop in degree of overall crystallinity. However, we note that such an observation could also be a result of changes in orientation of crystalline domain with respect to the film substrate, suggesting the crystallinity analysis using WAXS may not be conclusive. Nevertheless, the increased π-π stacking in the out-of-plane direction could be an advantage for high molecular weight DPP-TT-T as it would be expected to improve charge transport.[11]

Device Performance. The photovoltaic performance of DPP-TT-T fractions were evaluated in bulk heterojunction solar cells with a conventional device structure consisting of

ITO/PEDOT:PSS/Polymer:$PC_{71}BM$/Ca/Al. The current-voltage characteristics and external quantum efficiencies of the fractionated DPP-TT-T devices are presented in Figure 3 (left). The corresponding open circuit voltages, short circuit currents (J_{SC}), fill factors (FF) and PCE's are summarized in Table 2. Despite slightly higher V_{OC} and FF for low MW DPP-TT-T, the changes in PCE are mostly influenced by the differences in J_{SC}. It is apparent that devices fabricated with the low M_n (14 KDa) DPP-TT-T exhibit a relative poor power conversion efficiency (~ 2.2%), primarily due to their relatively low Jsc (5.3 mA cm^{-2}). The PCE of the devices increases to 5.4% when M_n is increased to 34 kDa, primarily due to an increase in J_{SC}. Further increase in M_n to 62KDa results in almost no difference in PCE due to a trade off between J_{SC} and FF.

External quantum efficiencies of DPP-TT-T based devices as a function of wavelength exhibit photocurrent generation from 350 nm to 800nm (Figure 3 (right)), matching well with UV-visible absorption range of the DPP-TT-T:$PC_{71}BM$ blend (see supporting information). Integration of these data yield calculated photocurrents in good agreement with those observed in Table 2 (within ± 3%). It is apparent that increasing polymer molecular weight increases the quantum efficiency of photocurrent generation following both fullerene (~ 350 - 600 nm) and DPP-TT-T (~ 600 - 850 nm) light absorption, with this increase being most pronounced for polymer light absorption, consistent with a number of other polymers reported elsewhere.[16, 20] All the polymer films exhibited similar optical absorbances (the blend with 14kDa DPP-TT-T, which exhibits the lowest J_{SC}, actually shows slightly stronger absorption in the polymer region - see supporting information); this increase in photocurrent density with increasing molecular weight therefore does not derive from differences in light harvesting, but rather from charge generation and collection.

Transient spectroscopy. Transient absorption spectroscopy was employed to investigate whether the increased photocurrent generation observed for the higher molecular weight devices could be explained by an increased charge separation yield. Transient absorption data were collected following excitation at 800 nm (corresponding to the polymer absorption maximum) and monitored at 1200 nm which, according to a previous study,[33] corresponds to DPP-TT-T polaron absorption, employing low excitation conditions such that the signal intensity scaled linearly with laser intensity. Figure 4 shows transient absorption traces for 1:2 ratio blend films of DPP-TT-T and $PC_{71}BM$. It is apparent that the initial amplitude of these traces (at ~ 0.17 μs), indicative of the yield of long lived DPP-TT-T polarons,[33] is increased by a factor of approximately 4 when the molecular weight of the polymer is increased from the lower, 14 kDa fraction to 62 kDa (Table 2). This trend qualitatively matches that in short circuit current, which suggests the increase in photocurrent with increasing molecular weight derives substantially from an increase in photoinduced charge generation.

Film morphology. One of the key determinants of charge generation is blend morphology. Atomic force microscopy was employed in order to investigate potential trends in film surface morphology with DPP-TT-T molecular weight, as shown in Figure 5. The phase segregation, defined by the bright and dark regions, of DPP-TT-T (14 kDa):$PC_{71}BM$ is on the order of approximately 200 nm. As the polymer molecular weight is increased, it is apparent that the domain size in the film becomes smaller. Whilst such topography images do not provide information on domain composition, and are moreover only a probe of surface rather than bulk morphology, and therefore only provide a limited viewpoint of film

morphology, it is apparent that the larger polymer molecular weight results in a finer nanomorphology, consistent with the better charge generation observed by TAS.

Further information of the correlation between polymer molecular weight and film morphology/exciton quenching was obtained from photoluminescence spectroscopy. We have previously shown that monitoring fullerene photoluminescence intensity can be correlated with PCBM domain length scale, with the observation of PCBM domains on the lengthscale of the PCBM singlet exciton diffusion length (~ 5nm[34]) or larger correlating with the observation of reduced PCBM photoluminescence quenching.[35] For the study presented herein, the samples were excited at 520 nm to excite $PC_{71}BM$ (the absorption of DPP-TT-T exhibits a minimum at this wavelength). All the results shown in Figure 6 are corrected for film absorbance. Pristine $PC_{71}BM$ films exhibit a photoluminescence peak at 707 nm, consistent with previous studies.[35] This emission intensity is reduced when the $PC_{71}BM$ is blended with DPP-TT-T, assigned to quenching of $PC_{71}BM$ singlet excitons due to charge separation following exciton diffusion to the PCBM:polymer interface. As shown in Figure 6, it is apparent that the efficiency of this photoluminescence quenching increases from 19% for the 14 kDa sample to 50% for 34 kDa and 68% for 62 kDa. This trend is consistent with the decrease in domain size observed in the AFM micrographs above with increasing molecular weight.

The agreement between the trends in EQE, transient absorption and photoluminescence quenching suggest that increasing the DPP-TT-T molecular weight can optimise the blend microstructure leading to better exciton dissociation and charge generation, and thus device performance (Table 1). In particular, the blend microstructure is optimised to improve the

exciton quenching by reducing the length scale of phase segregation between the polymer and $PC_{71}BM$.

Effects of thermal annealing.

We now consider the impact of thermal annealing upon the performance of DPP-TT-T:$PC_{71}BM$ devices in an attempt to optimize device efficiency. Annealing studies were conducted as a function of annealing time and temperature, molecular weight and for annealing before or after electrode deposition (pre- and post-annealing respectively). Typical data are shown in Figure 7.

Figure 7 (left) shows data as a function of annealing time at one temperature (80°C), using a 30 kDa DPP-TT-T fraction. Data are shown for pre- and post-annealing. Post-annealing was found to degrade device performance for all annealing times whilst pre-annealing improved PCE by up to 12% for annealing times up to 6 hours. Such behaviour is different from that observed for P3HT:PCBM devices where post-annealing is found to be more beneficial to device performance.[24] The loss in PCE by post-annealing in our case resulted from losses in Jsc and FF, probably due to anode delamination and/or active layer/anode inter-diffusion.[25, 26] Based on these results, the pre-annealing approach appears to be more appropriate for DPP-TT-T based OSC's, at least for the Ca/Al metal electrodes employed herein. Rather remarkably, after 250 hours of annealing at 80°C prior to electrode deposition, the DPP-TT-T:$PC_{71}BM$ solar cells retained an efficiency > 6 % (higher than the device without post-treatment).

Further experiments were carried out as a function of molecular weight and pre-annealing temperature. Typical data as a function of temperature for a 10 minute pre-annealing for

two different molecular weight DPP-TT-T's (M_n ~ 17 and 35 kDa) are shown in Figure 7 (right). The PCE of the 35 kDa DPP-TT-T devices were found to peak at a higher temperature (110°C), with a larger relative increase in performance than the 17 kDa devices. Overall, we found that the PCE of optimized DPP-TT-T (35 kDa) devices can achieve 6.6% by pre-annealing at 80 °C for 60 hours or 6.4 % by pre-annealing at 110 °C for 10 minutes. Regarding the latter, shorter annealing treatment, WAXS, AFM and PLQ studies were carried out to investigate the impact of thermal annealing upon film morphology. WAXS data indicate that the DPP-TT-T polymer becomes more crystalline after annealing (see Supporting Information). Whilst there were no obvious changes in terms of topography images measured by AFM, photoluminescence spectroscopy showed a small reduction in the efficiency of fullerene exciton quenching, implying a small increase in the fullerene domain size (Supporting Information).

Discussion

It is apparent from the results above that polymer molecular weight and thermal annealing can both impact upon the crystallinity as well as other features of blend microstructure (such as phase segregation and domain composition) for DPP-TT-T:$PC_{71}BM$ blends films, and thereby upon device performance. Increased polymer molecular weight and thermal annealing prior to electrode deposition are both shown to be capable of resulting in enhanced device efficiency. In general, disentangling the effects of crystallinity and the other features of blend microstructure upon device performance is challenging, not least as changes in crystallinity often result in changes in phase segregation. Crystallinity is a key determinant of not only film microstructure but also charge carrier mobilities and material energetics.[36, 37, 38, 19, 39, 40] Film microstructure can evolve both in terms of phase segregation

and in terms of domain composition, with the miscibility of polymer and fullerene being a key consideration.[27]

For the study reported herein, our AFM and photoluminescence quenching data indicate that increased polymer molecular weight results in a decrease in polymer crystalline domain size and an increased mixing of polymer:fullerene components. These trends correlate with an increase in exciton quenching efficiency, and are consistent with the increased yield of photoinduced charge carriers observed in our transient absorption data. These trends are consistent with the observed increase in photocurrent density with molecular weight. We have also observed this correlation can be extended to higher molecular weights using a DPP polymer with extended alkyl side groups (as reported elsewhere). Our observations herein are consistent with the trend of P3HT reported previously, where P3HT becomes more miscible with PCBM as molecular weight is increased.[17] Despite the limitations of WAXS, the data appears to suggest that the better miscibility of DPP-TT-T with fullerene at high molecular weight is due to the increased fraction of polymer amorphous phase, derived from a high degree of chain entanglements as in the model proposed by Westacott *et al*.[18]

Thermal annealing has previously been shown to enhance the performance of P3HT:PCBM devices[23, 42, 43] and correlated with increased P3HT crystallinity, as well as enhanced phase segregation. The enhanced crystallinity has been suggested to increase the energetic driving force for charge separation[44] as well as charge carrier mobilities,[45] whilst the increased phase segregation has been suggested to increase charge collection efficiency in particular through slower non-geminate recombination.[46] The annealing data we report herein for DPP-TT-T, whilst relatively limited in scope, suggests a similar behaviour to that of P3HT. The modestly enhanced crystallinity of DPP-TT-T after thermal annealing potentially improves

the charge separation efficiency as well as charge transportation, which outweighs the slightly reduced exciton dissociation efficiency and subsequently leads to increases in both short circuit current and PCE.[24] We also note that, at a fixed annealing period, a higher annealing temperature was required in order to maximize device performance for DPP-TT-T with higher molecular weight. This trend possibly results from the potentially stronger polymer-polymer interaction or reduced PCBM mobility in high molecular weight DPP-TT-T thin films.[11] We note however that material crystallinity is clearly not the only determinant of photocurrent density – both decreasing M_n and thermal annealing increase crystallinity, but only the later improves efficiency. As we discuss above, the loss of efficiency with decreasing M_n most probably derives from excessive increases in domain size.

We note that the enhancement in DPP-TT-T:$PC_{71}BM$ device performance with thermal annealing was only observed for annealing prior to metal electrode deposition. This contrasts to P3HT, where post-deposition annealing has been shown to give the best device performance.[24] Literature review suggests three possible reasons accounting for the DPP-TT-T device deterioration brought by post-annealing. Firstly, there could be some interdiffusion at the blend/anode interface if annealing is performed after anode coating.[26] This might have a negative influence on charge injection and therefore reduce the efficiency of charge collection at the electrode. Secondly, both the polymer and fullerene can adopt different diffusion under post-annealing treatment compared to pre-annealing.[47] Since the free volume at the interface is different in these cases (blend/nitrogen interface vs blend/calcium interface), polymer and fullerene diffusion could be different in the case of post-annealing and result in a sub-optimal unwanted morphology.[48,49] Lastly, anode delamination is also another potential concern which could lower the device performance.[43]

However we note a more detailed consideration of this point would require studies with different metal electrode, beyond the scope of this study.

The annealing data we report herein indicate that the morphology of the DPP-TT-T:PCBM blend films can be remarkably stable to prolonged, modest thermal annealing. In particular we observed that annealing at 80 °C for ~ 240 hours prior to electrode deposition resulted in negligible device performance degradation relative to devices with no pre-annealing. We note that this experiment was undertaken in a glove box under ambient lighting; it is possible that this impressive stability may result in part from light induced PCBM cross-linking.[50] Nevertheless this behaviour is substantially different from the thermal stability observed for most other donor polymers, where analogous thermal annealing typically results in rapid loss of device efficiency (with the most notable previous exception being P3HT).[28, 51] This observation of film thermal stability is promising for the practical device stability if the issue of thermal degradation associated with electrode deposition can be avoided. It is also important for high throughput device fabrication, where an annealing step is typically employed to accelerate the drying of the initially deposited blend film.

Conclusion

In summary, we have applied two optimisation approaches, tuning molecular weight and thermal annealing, to DPP-TT-T based devices which lead to positive effects on device performance. In both cases, these effects appear to be related to the changes in film crystallinity and microstructure, consistent with what have been previously reported for P3HT based devices. In the case of thermal annealing, we have demonstrated that by

carefully adjusting the annealing conditions, the device efficiency can be improved to 6.6%, and that the DPP-TT-T:$PC_{71}BM$ blend morphology is remarkably stable to prolonged modest annealing, thereby emphasing the potential importance of this polymer class for technological application.

Acknowledgements

Funding from Solvay SA and the EPSRC projects EP/J500021 and EP/I019278 is gratefully acknowledged.

Dedications

Device fabrications were performed by Z.H. and P.S.T. Transient spectroscopy measurements were performed by E.C.F. and S.D.. Morphology studies were performed by Y.W.S and Z.H. Material synthesis and fractionation were performed by H.B., W.Z. and I.M.. Data analysis was performed by Z.H. and S.D. The project planning, experiment designs as well as manuscript preparation were contributed by J.R.D. and I.M..

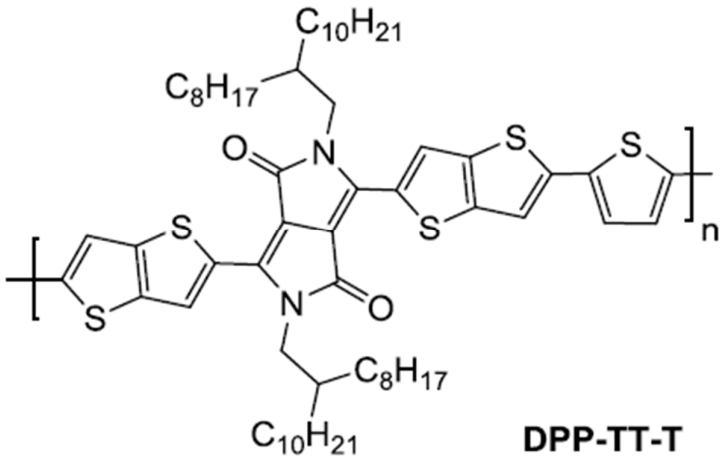

Figure 1: Chemical structure of DPP-TT-T.

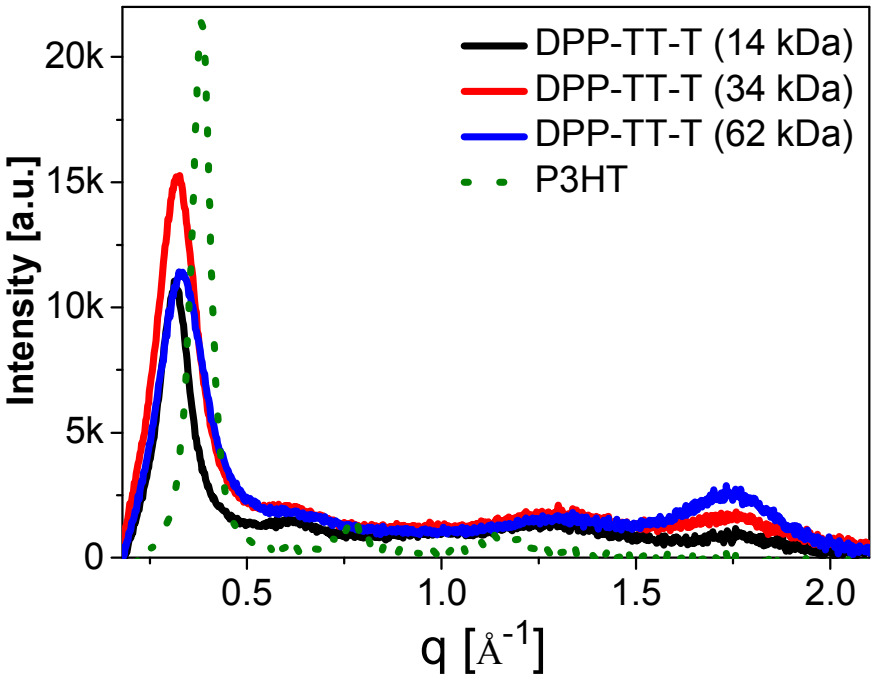

Figure 2: Wide angle X-ray scattering (WAXS) of pristine DPP-TT-T polymers with different molecular weight, as well as that of a P3HT reference film. The samples were prepared using drop casting.

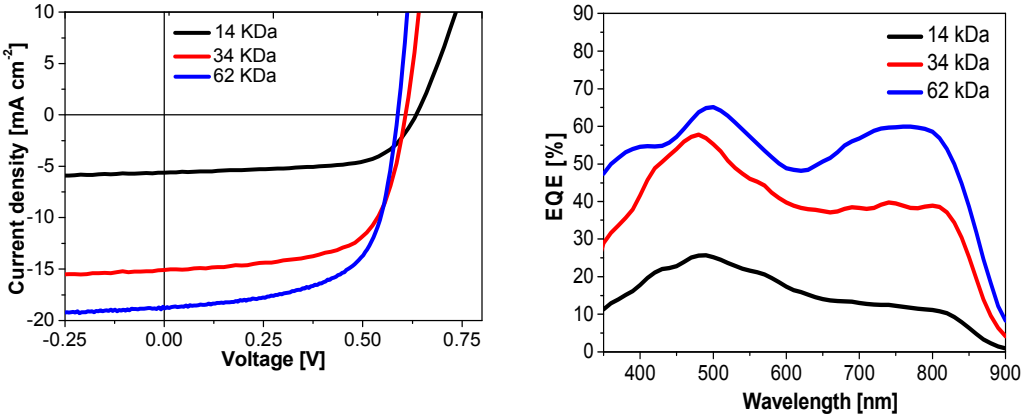

Figure 3: Current-voltage characteristics (left) of the DPP-TT-T based devices with different polymer molecular weights under AM 1.5 simulated irradiation (100 mW cm^{-2}), and the corresponding external quantum efficiencies (right.)

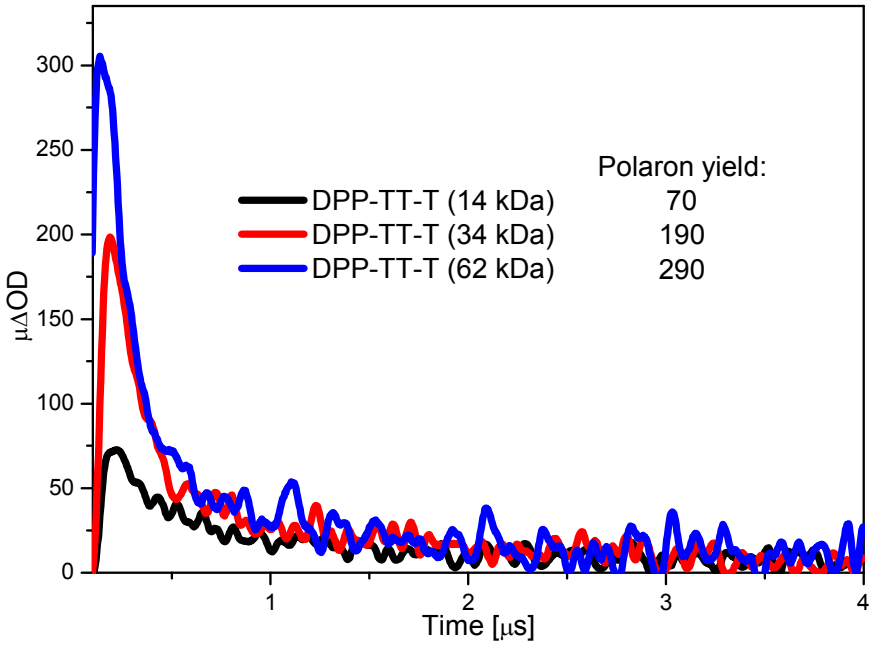

Figure 4: Transient absorption decays obtained by exciting blend films of DPP-TT-T1:2 $PC_{71}BM$: DPP-TT-T with different molecular weights at 800 nm with 2 μJ cm^{-2}, probing at 1200 nm.

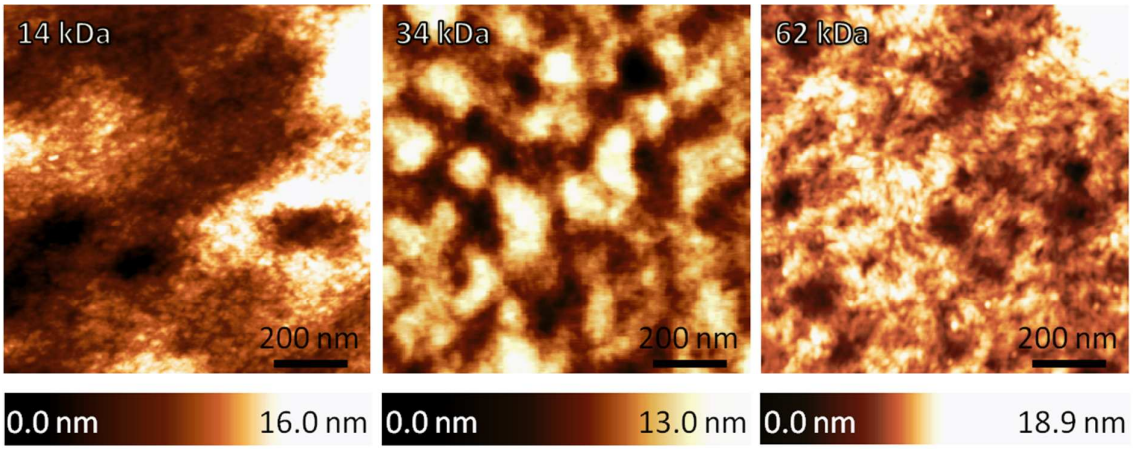

Figure 5: Topography images of DPP-TT-T:$PC_{71}BM$ films (1:2) with different polymer molecular weight measured by atomic force microscopy.

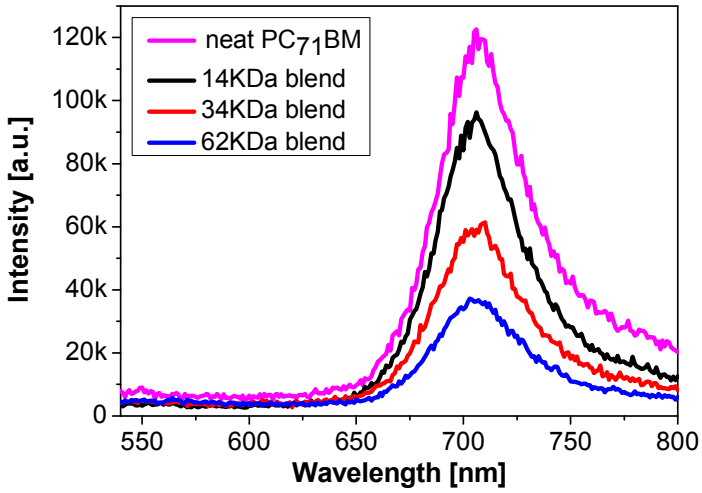

Figure 6: Photoluminescence spectra of DPP-TT-T:$PC_{71}BM$ thin films with different polymer molecular weights, and a neat $PC_{71}BM$ filmThe PL data were obtained at 520nm excitation without correction for detector response.

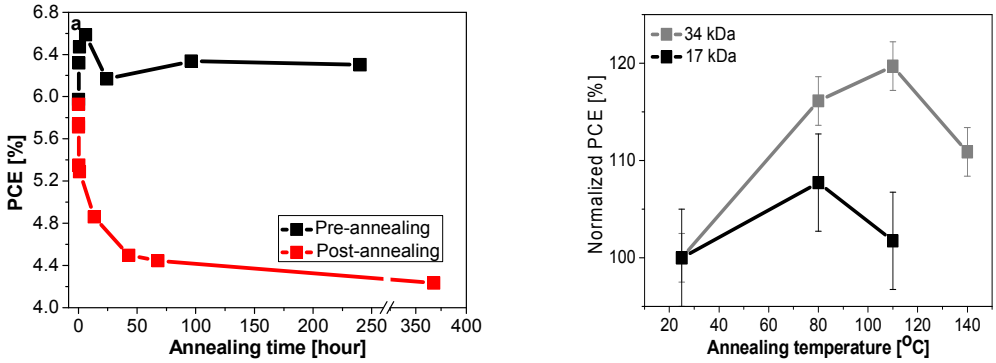

Figure 7: Thermal annealing study on DPP-TT-T based devices. Evolution of device efficiencies with time from pre-annealing (black) and post annealing (red) at 90 °C using DPP-TT-T with M_n ~ 17kDa (left). Evolution of device efficiencies with pre-annealing temperature for DPP-TT-T with two different molecular weights (17 and 34 kDa) (right), with.the annealing time fixed at 10 minutes.

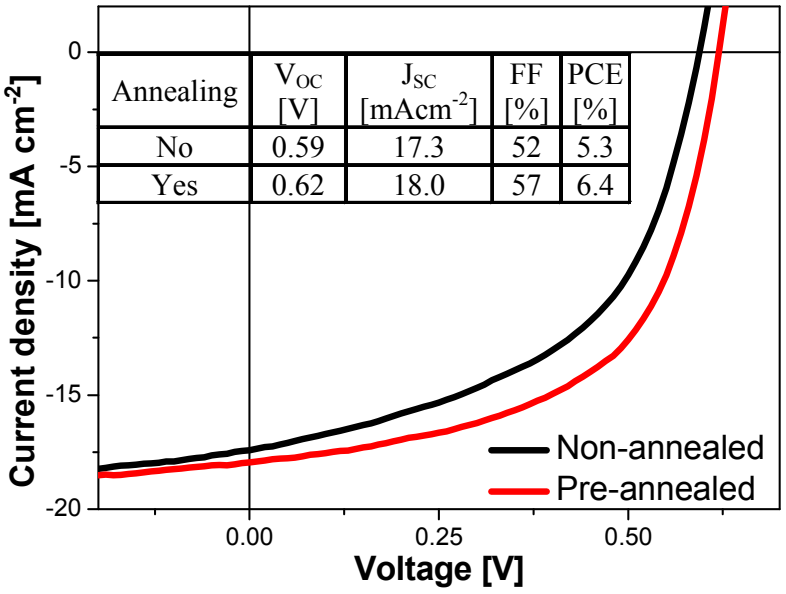

Figure 8: Current-voltage characteristics of pristine (black) and annealed (red) DPP-TT-T devices, with inserted table showing the device parameters using 35 kDa DPP-TT-T. The 'pre-annealed device subjected was annealed at 80 °C for 6 hours prior to metal electrode deposition.

Table 1: Diffraction strengths extracted by the integrating the WAXS peaks from Figure 1 and correcting by the drop-cast film thickness. The overall diffraction strength is the sum of the diffraction strength from the lamellar packing signals and that from π-π stacking signals.

Polymer	Diffraction strength of Lamellar packing	Diffraction strength of π-π stacking	Overall diffraction strength
DPP-TT-T (14 kDa)	272	68	340
DPP-TT-T (34 kDa)	225	66	291
DPP-TT-T (62 kDa)	203	99	302
P3HT	1042	-	1042

Table 2: Photovoltaic parameters of DPP-TT-T based devices with different polymer molecular weight, TAS signal taken at 0.17 μs (Fig 6) and PL quenching calculated from the PL measurements (Fig 4).

Molecular weight	V_{oc} [±20mV]	J_{sc} [±0.5mA cm^{-2}]	FF [±5%]	PCE [±0.3%]	TAS amplitude [μOD]	PL quenching [%]
14KDa	630	5.3	64	2.2	70	19
34KDa	600	13.9	65	5.4	190	50
62KDa	600	16.0	56	5.4	290	68

References

1. N. C. Miller, E. Cho, R. Gysel, C. Risko, V. Coropceanu, C. E. Miller, S. Sweetnam, A. Sellinger, M. Heeney, I. McCulloch, J. L. Bredas, M. F. Toney and M. D. McGehee, *Adv Energy Mater*, 2012, **2**, 1208-1217.
2. Y. Y. Liang, Z. Xu, J. B. Xia, S. T. Tsai, Y. Wu, G. Li, C. Ray and L. P. Yu, *Adv Mater*, 2010, **22**, E135-+.
3. S. Y. Qu and H. Tian, *Chem Commun*, 2012, **48**, 3039-3051.
4. D. Chandran and K. S. Lee, *Macromol Res*, 2013, **21**, 272-283.
5. H. Bronstein, Z. Y. Chen, R. S. Ashraf, W. M. Zhang, J. P. Du, J. R. Durrant, P. S. Tuladhar, K. Song, S. E. Watkins, Y. Geerts, M. M. Wienk, R. A. J. Janssen, T. Anthopoulos, H. Sirringhaus, M. Heeney and I. McCulloch, *J Am Chem Soc*, 2011, **133**, 3272-3275.

6. H. Bronstein, E. Collado-Fregoso, A. Hadipour, Y. W. Soon, Z. Huang, S. D. Dimitrov, R. S. Ashraf, B. P. Rand, S. E. Watkins, P. S. Tuladhar, I. Meager, J. R. Durrant and I. McCulloch, *Advanced Functional Materials*, 2013, n/a-n/a.
7. I. Meager, R. S. Ashraf, S. Mollinger, B. C. Schroeder, H. Bronstein, D. Beatrup, M. S. Vezie, T. Kirchartz, A. Salleo, J. Nelson and I. McCulloch, *J Am Chem Soc*, 2013, **135**, 11537-11540.
8. H. X. Zhou, L. Q. Yang and W. You, *Macromolecules*, 2012, **45**, 607-632.
9. H. J. Son, B. Carsten, I. H. Jung and L. P. Yu, *Energ Environ Sci*, 2012, **5**, 8158-8170.
10. Y. W. Soon, S. Shoaee, R. S. Ashraf, H. Bronstein, B. C. Schroeder, W. Zhang, Z. Fei, M. Heeney, I. McCulloch and J. R. Durrant, *Adv Funct Mater*, 2013, 1474-1482.
11. P. Schilinsky, U. Asawapirom, U. Scherf, M. Biele and C. J. Brabec, *Chemistry of Materials*, 2005, **17**, 2175-2180.
12. B. N. Kang, L. D. Wang, Y. Yang and Y. Qiu, *Chinese Sci Bull*, 2004, **49**, 2259-2261.
13. S. Wakim, S. Beaupre, N. Blouin, B. R. Aich, S. Rodman, R. Gaudiana, Y. Tao and M. Leclerc, *J Mater Chem*, 2009, **19**, 5351-5358.
14. T. Y. Chu, J. P. Lu, S. Beaupre, Y. G. Zhang, J. R. Pouliot, J. Y. Zhou, A. Najari, M. Leclerc and Y. Tao, *Adv Funct Mater*, 2012, **22**, 2345-2351.
15. E. Y. Park, J. Jung, S. Y. Nam, P. S. Kim, J. Y. Lee, J. Lee, W. S. Shin, S. J. Moon, C. Lee and S. C. Yoon, *J Nanosci Nanotechno*, 2012, **12**, 4256-4260.
16. J. J. Intemann, K. Yao, H. L. Yip, Y. X. Xu, Y. X. Li, P. W. Liang, F. Z. Ding, X. S. Li and A. K. Y. Jen, *Chemistry of Materials*, 2013, **25**, 3188-3195.
17. C. Nicolet, D. Deribew, C. Renaud, G. Fleury, C. Brochon, E. Cloutet, L. Vignau, G. Wantz, H. Cramail, M. Geoghegan and G. Hadziioannou, *J Phys Chem B*, 2011, **115**, 12717-12727.
18. P. Westacott, J. R. Tumbleston, S. Shoaee, S. Fearn, J. H. Bannock, J. B. Gilchrist, S. Heutz, J. deMello, M. Heeney, H. Ade, J. Durrant, D. S. McPhail and N. Stingelin, *Energ Environ Sci*, 2013, **6**, 2756-2764.
19. S. J. Li, S. S. Wang, B. H. Zhang, F. Ye, H. W. Tang, Z. B. Chen and X. N. Yang, *Org Electron*, 2014, **15**, 414-427.
20. J. C. Bijleveld, A. P. Zoombelt, S. G. J. Mathijssen, M. M. Wienk, M. Turbiez, D. M. de Leeuw and R. A. J. Janssen, *J Am Chem Soc*, 2009, **131**, 16616-16617.
21. K. H. Hendriks, G. H. L. Heintges, V. S. Gevaerts, M. M. Wienk and R. A. J. Janssen, *Angew Chem Int Edit*, 2013, **52**, 8341-8344.
22. W. L. Ma, C. Y. Yang, X. Gong, K. Lee and A. J. Heeger, *Adv Funct Mater*, 2005, **15**, 1617-1622.
23. P. E. Keivanidis, T. M. Clarke, S. Lilliu, T. Agostinelli, J. E. Macdonald, J. R. Durrant, D. D. C. Bradley and J. Nelson, *J Phys Chem Lett*, 2010, **1**, 734-738.
24. G. Li, V. Shrotriya, Y. Yao and Y. Yang, *J Appl Phys*, 2005, **98**, 043704/1-043704/5.
25. J. Y. Kim, S. Noh, J. Kwak and C. Lee, *J Nanosci Nanotechno*, 2013, **13**, 3360-3364.
26. F. Li, J. Zhao, K. Yao and Y. W. Chen, *Chem Phys Lett*, 2012, **553**, 36-40.
27. J. Bisquert and G. Garcia-Belmonte, *J Phys Chem Lett*, 2011, **2**, 1950-1964.
28. Z. M. Beiley, E. T. Hoke, R. Noriega, J. Dacuna, G. F. Burkhard, J. A. Bartelt, A. Salleo, M. F. Toney and M. D. McGehee, *Adv Energy Mater*, 2011, **1**, 954-962.
29. J. C. Guo, Y. Y. Liang, J. Szarko, B. Lee, H. J. Son, B. S. Rolczynski, L. P. Yu and L. X. Chen, *J Phys Chem B*, 2010, **114**, 4746-4746.
30. T. M. Clarke, A. Ballantyne, S. Shoaee, Y. W. Soon, W. Duffy, M. Heeney, I. McCulloch, J. Nelson and J. R. Durrant, *Adv Mater*, 2010, **22**, 5287-5291.

31. R. S. Ashraf, B. C. Schroeder, H. A. Bronstein, Z. G. Huang, S. Thomas, R. J. Kline, C. J. Brabec, P. Rannou, T. D. Anthopoulos, J. R. Durrant and I. McCulloch, *Adv Mater*, 2013, **25**, 2029-2034.
32. J. Rivnay, S. C. B. Mannsfeld, C. E. Miller, A. Salleo and M. F. Toney, *Chem Rev*, 2012, **112**, 5488-5519.
33. H. Bronstein, E. Collado-Fregoso, A. Hadipour, Y. W. Soon, Z. Huang, S. D. Dimitrov, R. S. Ashraf, B. P. Rand, S. E. Watkins, P. S. Tuladhar, I. Meager, J. R. Durrant and I. McCulloch, *Adv Funct Mater*, 2013, **23**, 5647-5654.
34. S. Cook, A. Furube, R. Katoh and L. Y. Han, *Chem Phys Lett*, 2009, **478**, 33-36.
35. S. D. Dimitrov, C. B. Nielsen, S. Shoaee, P. S. Tuladhar, J. P. Du, I. McCulloch and J. R. Durrant, *J Phys Chem Lett*, 2012, **3**, 140-144.
36. C. H. Woo, B. C. Thompson, B. J. Kim, M. F. Toney and J. M. J. Frechet, *J Am Chem Soc*, 2008, **130**, 16324-16329.
37. G. Defieuw, G. Groeninckx and H. Reynaers, *Polymer*, 1989, **30**, 2164-2169.
38. R. G. Alamo, J. D. Londono, L. Mandelkern, F. C. Stehling and G. D. Wignall, *Macromolecules*, 1994, **27**, 411-417.
39. H. J. Chiu, H. L. Chen and J. S. Lin, *Polymer*, 2001, **42**, 5749-5754.
40. F. P. V. Koch, J. Rivnay, S. Foster, C. Muller, J. M. Downing, E. Buchaca-Domingo, P. Westacott, L. Y. Yu, M. J. Yuan, M. Baklar, Z. P. Fei, C. Luscombe, M. A. McLachlan, M. Heeney, G. Rumbles, C. Silva, A. Salleo, J. Nelson, P. Smith and N. Stingelin, *Prog Polym Sci*, 2013, **38**, 1978-1989.
41. S. D. Dimitrov, Z. Huang, F. Deledalle, C. B. Nielsen, B. C. Schroeder, R. S. Ashraf, S. Shoaee, I. McCulloch and J. R. Durrant, *Energ Environ Sci*, 2014, 1037-1043.
42. T. J. Savenije, J. E. Kroeze, X. N. Yang and J. Loos, *Adv Funct Mater*, 2005, **15**, 1260-1266.
43. D. Chirvase, J. Parisi, J. C. Hummelen and V. Dyakonov, *Nanotechnology*, 2004, **15**, 1317-1323.
44. T. M. Clarke, F. C. Jamieson and J. R. Durrant, *J Phys Chem C*, 2009, **113**, 20934-20941.
45. M. Nakazono, T. Kawai and K. Yoshino, *Chemistry of Materials*, 1994, **6**, 864-870.
46. R. Hamilton, C. G. Shuttle, B. O'Regan, T. C. Hammant, J. Nelson and J. R. Durrant, *J Phys Chem Lett*, 2010, **1**, 1432-1436.
47. H. Y. Lu, B. Akgun and T. P. Russell, *Adv Energy Mater*, 2011, **1**, 870-878.
48. M. Campoy-Quiles, T. Ferenczi, T. Agostinelli, P. G. Etchegoin, Y. Kim, T. D. Anthopoulos, P. N. Stavrinou, D. D. C. Bradley and J. Nelson, *Nat Mater*, 2008, **7**, 158-164.
49. X. N. Yang, A. Alexeev, M. A. J. Michels and J. Loos, *Macromolecules*, 2005, **38**, 4289-4295.
50. Z. Li, H. C. Wong, Z. G. Huang, H. L. Zhong, C. H. Tan, W. C. Tsoi, J. S. Kim, J. R. Durrant and J. T. Cabral, *Nat Commun*, 2013, **4**.
51. N. C. Cates, R. Gysel, J. E. P. Dahl, A. Sellinger and M. D. McGehee, *Chemistry of Materials*, 2010, **22**, 3543-3548.

Table of content entry

Performance of bulk heterojunction solar cells based on a novel donor polymer DPPTT-T was optimised using two different approaches, namely tuning molecular weight and thermal annealing.